Direct Flux Field Oriented Control of IPM Drives with Variable DC-Link in the Field-Weakening Region

# Direct Flux Field-Oriented Control of IPM Drives With Variable DC Link in the Field-Weakening Region

Gianmario Pellegrino, *Member, IEEE*, Eric Armando, and Paolo Guglielmi, *Member, IEEE*

***Abstract*—This paper presents the direct flux control of an interior permanent-magnet (IPM) motor drive in the field-weakening region. The output torque is regulated by the coordinated control of the stator flux amplitude and the current component in quadrature with the flux, and it is implemented in the stator flux reference frame. The control system guarantees maximum torque production taking into account voltage and current limits, in particular in case of large dc-link variations. The field-oriented control does not necessarily require an accurate magnetic model of the IPM motor, and it is able to exploit the full inverter voltage at different dc-link levels with no additional voltage control loop. The feasibility of the proposed control method is investigated in discrete-time simulation, then tested on a laboratory rig, and finally implemented on board of an electric scooter prototype. The motor under test is an IPM permanent-magnet-assisted synchronous reluctance machine, with high-saliency and limited permanent-magnet flux.**

***Index Terms*—Direct flux control, motor drives control, synchronous motor drives, variable-speed drives, wide speed range.**

## I. Introduction

THE INTERIOR permanent-magnet (IPM) motor drives are particularly adapted to applications where a constant-power speed range is required, such as vehicle propulsion and machine tools, for their good flux-weakening capability [1], [2].

The flux weakening capability of an IPM motor drive depends on the machine design, and it is a tradeoff between the rotor saliency and permanent-magnet quantity [3]. Once the IPM motor is purposely designed for flux weakening [4], [5], a proper control strategy is needed to obtain the maximum output torque given the inverter size (maximum voltage and maximum current).

Most of the vector control schemes for IPM motor drives are based on the control of the current vector in the rotor synchronous frame $(d, q)$. In that case, field weakening is obtained by current reference tables calculated according to the motor magnetic model [6], [7]. The effectiveness of this approach relies on the accurate identification of the machine model. Moreover, the current references are necessarily calculated for a determined dc-link voltage level. In case of a variable dc link, an additional voltage loop is needed [8], [9], to correct the calculated current reference values.

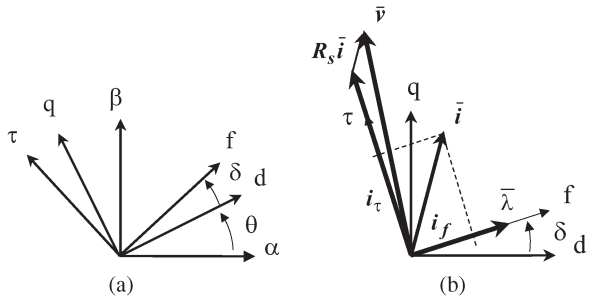


Fig. 1. Definition of the reference frames and IPM machine vector diagram. (a) $\alpha\beta$: stator frame; $dq$: rotor frame; $f\tau$: field-oriented frame. (b) Steady-state vector diagram.

This paper proposes a direct flux control implemented in the $f$, $\tau$ reference frame aligned with the stator flux and shown in Fig. 1(a). The output torque is regulated by controlling the stator flux amplitude $\lambda$ and the current component in quadrature with the flux $i_\tau$ by means of the $f$ and $\tau$ voltage components, respectively. The proposed algorithm permits the exploitation of the maximum torque profile of the IPM motor drive, also with a variable dc link. A suitable flux observer scheme is needed for control orientation and accurate flux control.

The adoption of a flux observer has been proposed in the literature for IPM motor drives [10]–[12], to overcome the limitations of current control in field weakening. For example, the flux amplitude can be controlled by an additional flux loop, like for induction motor (IM) drives [13]–[15]. Another idea is to control the components of the flux vector instead of the components of the current [10], e.g., the $\lambda_d$, $i_q$ control proposed in [16]. Direct flux field-oriented control has been rarely adopted. In [17] and [18], it is proposed for synchronous reluctance machines, and in [19], [20] for IPM motor drives.

The field-oriented direct flux control proposed here has some aspects in common with the stator flux-oriented control of IM drives that has good performance in flux weakening [21]. The direct control of the flux amplitude can also remind the direct-torque-control (DTC) approach; however, there is no current loop in DTC schemes [22], while here, the $i_\tau$ component is

Paper 2008-IDC-138.R1, presented at the 2007 Industry Applications Society Annual Meeting, New Orleans, LA, September 23–27, and approved for publication in the IEEE TRANSACTIONS ON INDUSTRY APPLICATIONS by the Industrial Drives Committee of the IEEE Industry Applications Society. Manuscript submitted for review November 6, 2008 and released for publication March 11, 2009. First published July 14, 2009; current version published September 18, 2009.

The authors are with the Department of Electrical Engineering, Politecnico di Torino, 10129 Turin, Italy (e-mail: gianmario.pellegrino@polito.it).

Color versions of one or more of the figures in this paper are available online at http://ieeexplore.ieee.org.

Digital Object Identifier 10.1109/TIA.2009.2027167

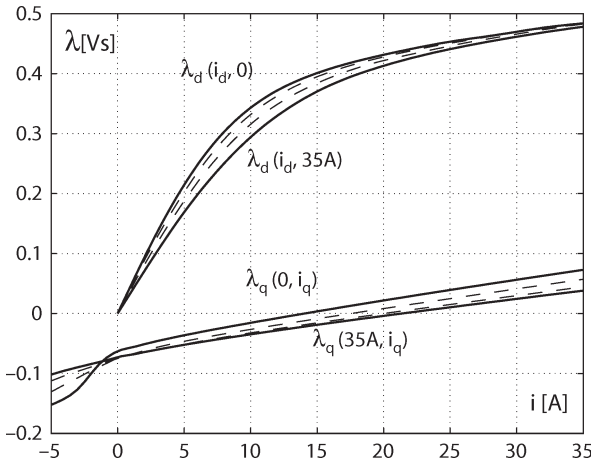


Fig. 2. Experimental magnetic curves of the motor under test.

controlled in closed loop and suitably limited for obtaining exact maximum current operation.

In this paper, the control is implemented on the IPM motor traction drive for an electric scooter prototype [23]. The adopted motor is of the permanent-magnet-assisted synchronous reluctance (PMASR) type, as will be explained in the following section. Test results on a laboratory test rig and on the vehicle are provided.

This paper is organized as follows. Section II is dedicated to the motor model in the field-oriented frame and the definition of the control variables $\lambda$ and $i_\tau$. In Section III, the maximum torque field-weakening control is reviewed and the control trajectories are represented in the flux plane other than in the more usual current plane. In Section IV, the proposed control scheme is presented and investigated. In Section V, simulated and experimental results are provided. In the Appendix, the ratings of the IPM motor drive and of the electric scooter prototype are reported.

## II. Motor Model in the Field-Oriented Frame

The motor under test, whose data are reported in Table I in the Appendix, has been characterized by means of the procedure described in [24]. The experimental magnetic curves are shown in Fig. 2. Cross-saturation effect is evidenced by the different $\lambda_d$ and $\lambda_q$ curves for different cross-current values. The different slopes of $d$—and $q$—flux curves state for the high-saliency ratio of the motor, while the permanent-magnet flux ($0.07\ \mathrm{V}\cdot\mathrm{s}$ at $i_d = i_q = 0$) appears to be little respect to the $d$-axis flux. The rated machine flux is $0.405\ \mathrm{V}\cdot\mathrm{s}$, as defined in Section III. This kind of motors, with a little magnets flux and a high saliency, are also called PMASR motors [25], for which the $d$–$q$ frame is shown in Fig. 3, the same as for Synchronous Reluctance machines. The reference axes that are typical of IPM motor drives are shown as $d'$–$q'$ in Fig. 3.

### A. Rotor Frame $(d, q)$

The IPM motor model in $(d, q)$ is described by (1)–(3). According to the adopted axes orientation, the permanent motor

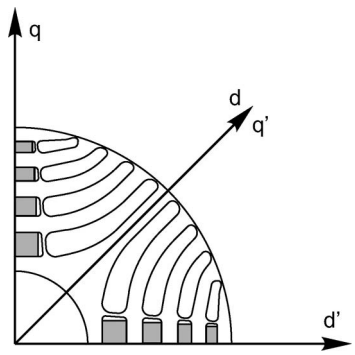


Fig. 3. Adopted $(d$–$q)$ frame and standard frame for IPM motors $(d'$–$q')$.

(PM) flux is aligned to the $q$-axis and it is negative

$$\overline{v}_{dq} = R\bar{i}_{dq} + \frac{d\overline{\lambda}_{dq}}{dt} + j\omega\overline{\lambda}_{dq} \tag{1}$$

$$\overline{\lambda}_{dq} = \begin{vmatrix} L_d & 0 \\ 0 & L_q \end{vmatrix} \cdot \bar{i}_{dq} - \begin{vmatrix} 0 \\ \lambda_m \end{vmatrix} \tag{2}$$

$$\frac{T}{3/2p} = \lambda_d i_q - \lambda_q i_d \tag{3}$$

where

| | |
|---|---|
| $p$ | pole-pairs; |
| $R$ | stator resistance; |
| $L_d$, $L_q$ | inductances of maximum and minimum permeance axes; |
| $\lambda_m$ | PM flux; |
| $T$ | electromagnetic torque. |

### B. Flux-Oriented Frame $(f, \tau)$

The flux-oriented reference frame $(f, \tau)$, where $f$ stands for *flux* and $\tau$ stands for *torque*, is shown in Fig. 1(a). In the new coordinates, the two state variables $\lambda$ and $\delta$ are decoupled between the $f$ and $\tau$ components in the voltage equation (4)

$$\overline{v}_{f\tau} = R\bar{i}_{f\tau} + \frac{d}{dt}\begin{vmatrix} \lambda \\ 0 \end{vmatrix} + \lambda \begin{vmatrix} 0 \\ \omega + \frac{d\delta}{dt} \end{vmatrix} \tag{4}$$

$$\frac{T}{3/2p} = \frac{1}{L_q} \cdot \left\{ \left(1 - \frac{L_q}{L_d}\right) \lambda^2 \frac{\sin 2\delta}{2} + \lambda_m \lambda \cos\delta \right\} \tag{5}$$

$$\frac{T}{3/2p} = \lambda \cdot i_\tau \tag{6}$$

$$\overline{\lambda}_{dq} = \lambda \cdot \begin{vmatrix} \cos\delta \\ \sin\delta \end{vmatrix}. \tag{7}$$

The torque expression (5) has been obtained by substituting (2) and (7) in (3). $\lambda$ is the stator flux amplitude and $\delta$ is the phase angle respect to the $d$ axis. The torque-current component $i_\tau$ has been introduced to obtain a simple the expression of the torque (6) respect to the one in $\lambda$, $\delta$ (5).

### C. State Variables: $\lambda$, $i_\tau$

In the voltage equation (4), the two state variables are the flux amplitude and phase angle $\lambda$ and $\delta$. However, the expression of torque in terms of $\lambda$, $\delta$ is quite complicate and achieving a linear and decoupled control of the torque by the control of $\lambda$ and $\delta$ is

not straightforward (5). The substitution of the flux phase angle $\delta$ with the new variable $i_\tau$, that is the current component in quadrature with the flux, makes the control of torque linear and decoupled between the two controlled variables $\lambda$ and $i_\tau$. The voltage equation in $(\lambda, i_\tau)$ is reported in

$$\frac{d}{dt}\begin{vmatrix}\lambda\\ i_\tau\end{vmatrix} \cong \begin{vmatrix}1 & 0\\ \frac{k}{L_q} & \frac{b}{L_q}\end{vmatrix}\cdot\begin{vmatrix}v_f\\ v_\tau-\omega\lambda\end{vmatrix} \tag{8}$$

where

$$k = k(\delta) = \frac{1}{2}\left(1-\frac{L_q}{L_d}\right)\sin 2\delta \tag{9}$$

$$b = b(\lambda,\delta) = \frac{L_q}{\lambda^2}\left(\frac{dT}{d\lambda}\right)_{\lambda=\text{const}} = \left(1-\frac{L_q}{L_d}\right)\cos 2\delta - \frac{\lambda_m}{\lambda}\sin\delta. \tag{10}$$

The resistive drops have been disregarded in (8). The variable factors $b(\lambda,\delta)$ and $k(\delta)$ are two functions of the machine magnetic state. This means that the control of the $i_\tau$ current component will be influenced by the actual size and position of the flux as better explained in Section IV.

## III. Maximum Torque Field-Weakening Control

Most of IPM motor drives make use of the current vector control. In that case, the strategy for maximum-torque in field weakening is graphically represented by a trajectory in the $(i_d, i_q)$ plane [3], [7], [8], [26]. The ideal current path for maximum torque control $(A \to B \to C)$ is shown in Fig. 4(a) for the drive under test. As mentioned in Section II, the $dq$ axes are rotated with respect to the ones adopted in the referenced papers.

For describing the direct-flux control, the trajectory $A \to B \to C$ is usefully represented in the $(\lambda_d, \lambda_q)$ plane. Some remarks about the characteristic curves of the drive in the two different planes are given in the followings.

With reference to Fig. 4, constant current contours are represented by circles in the current plane (a) and by ellipses with a vertical offset in the flux plane (b). Analogously, constant flux (i.e., voltage) contours are offset ellipses in the current plane and circles in the flux plane.

The maximum torque per ampere (MTPA) trajectory defines the control points for achieving the maximum torque at any given current, that means the minimum copper loss per torque. The intersection of the MTPA curve and the rated inverter current circle determines the maximum torque of the drive.

The maximum torque per voltage (MTPV) trajectory gives the maximum torque at any flux, and it is the curve that limits the maximum torque strategy at high speed. According to the definition of the $b$ factor (10), the MTPV curve corresponds to the condition $b = 0$, as evidenced by the label in Fig. 4. In the proposed direct flux control, the MTPV trajectory represents a boundary outside which torque control loses stability, as investigated in Section IV.

The description of how the $A \to B \to C$ trajectory has been obtained is briefly reviewed in the following, with reference to

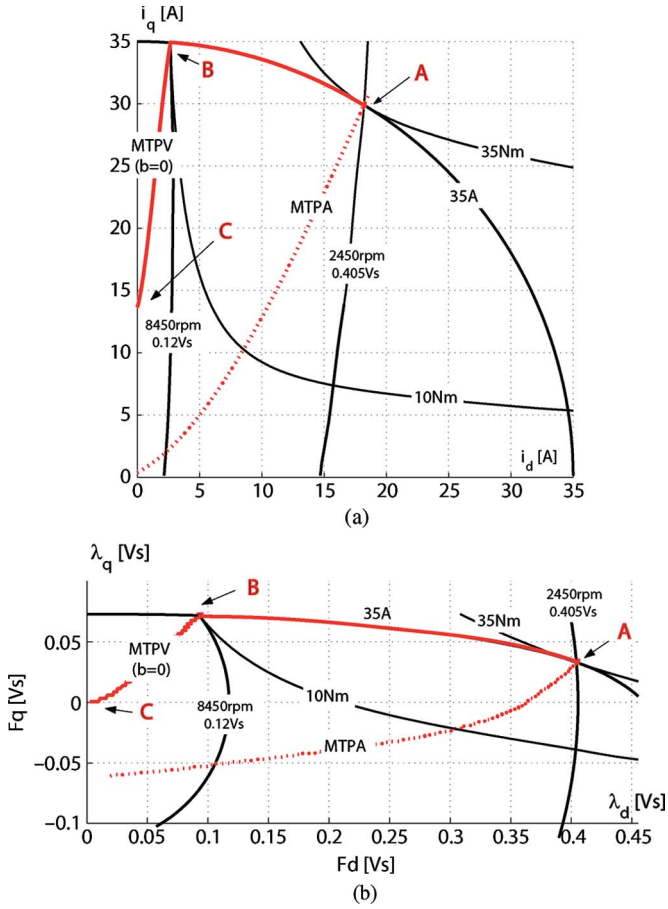


Fig. 4. Current and flux trajectories for maximum torque control. (a) Current coordinates. (b) Flux coordinates.

the corresponding motor speed intervals. The maximum torque trajectory is independent on the type of control (current control or direct flux control). The inverter ratings are summarized by the current and voltage limits $I_{\max}$ and $V_{\max}$, referenced in Table I in the Appendix.

1) Point $A$ $(0 \div \omega_A)$: It is the intersection between the MTPA curve and the $I_{\max}$ circle. Nominal torque and flux follow: $T_{\text{nom}} = 35$ N · m, $\lambda_{\text{nom}} = \lambda_A = 0.405$ V · s, as well as base speed $\omega_A = 2450$ r/min, calculated at $V_{\max}$, $\lambda_{\text{nom}}$.
2) Trajectory $A \to B$ $(\omega_A \div \omega_B)$: It is the current and voltage-limited region, along the $I_{\max}$ circle that intersects the MTPV curve in point B. The flux in B is $\lambda_B = 0.12$ V · s. The speed $\omega_B = 8450$ r/min is calculated according to $V_{\max}$, $\lambda_B$.
3) Trajectory $B \to C$ $(\omega_B \div \infty)$: It is the voltage-limited region. The drive operates on the MTPV curve, with no theoretical speed limit.

The maximum torque and power performance corresponding to Fig. 4(a) and (b) diagrams is then shown in Fig. 5. At high speed and high level of flux weakening, the harmonic iron losses can influence the output torque significantly. This effect is not taken into account in the output torque forecast of Fig. 5; thus, the actual torque profile will be lower than expected.

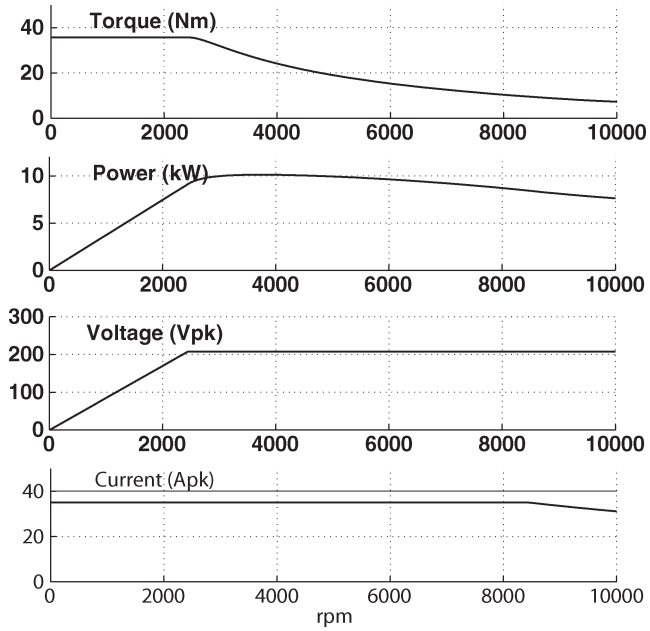


Fig. 5. Maximum torque and power performance of the IPM drive.

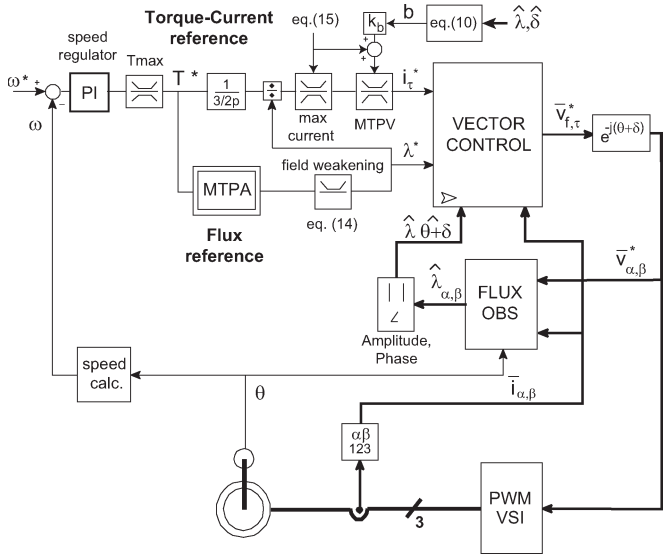


Fig. 6. Proposed control scheme. Stator flux frame $(f, \tau)$. Controlled state variables: $\lambda$, $i_\tau$.

## IV. Description of the Control Scheme

The proposed control scheme is shown in Fig. 6. The flux reference $\lambda^*$ is determined by the requested torque according to the MTPA curve, and the corresponding $i_\tau^*$ value is calculated coherently with the torque expression (6).

The *Flux-Weakening* block limits the reference flux above the base speed $(\omega > \omega_A)$, before the reference $i_\tau^*$ is calculated. The *VECTOR CONTROL* block consists of the two proportional-integral (PI) regulators shown in Fig. 7. The limitation block on $i_\tau^*$ ensures the respect of the inverter current limit $I_{\max}$ and the $b > 0$ stability. About the PI regulators, only the proportional term is shown in Fig. 7, to put in evidence the respective closed loop bandwidths $(\omega_b)_f$ and $(\omega_b)_\tau$.

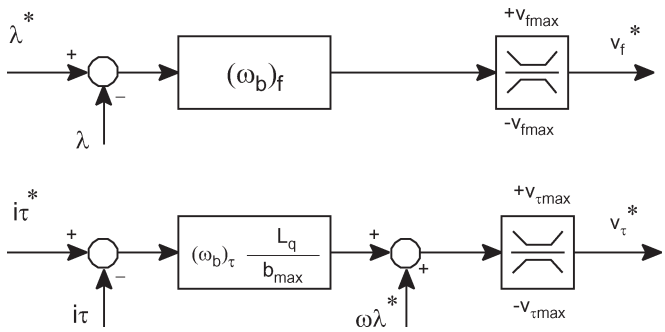


Fig. 7. $\lambda$ and $i_\tau$ regulators. Closed-loop bandwidth $(\omega_b)_f$ and $(\omega_b)_\tau$ are put in evidence in the proportional regulator.

### A. Flux Regulator

According to (8), the flux amplitude can be controlled by means of the $v_f$ voltage, with no influence by the $\tau$—components. The flux loop response is very fast: Apart from the limitation due to pulsewidth modulation (PWM) time discretization, the flux bandwidth is limited only by the dynamics of the flux estimator. With most of the flux observers in the literature [10]–[12], bandwidths on the order of kilohertz or more are possible.

### B. $i_\tau$ Regulator

The control of the $i_\tau$ current is obtained through the $v_\tau$ voltage component, but with less ideal properties respect to $\lambda$. First of all, there is an interaction with the flux loop given by the $v_f$ and $\omega\lambda$ terms in (8). This interaction is dynamically tackled by the fast response of the proportional $i_\tau$ regulator. The integrative regulator then compensates the $v_f$ disturbance at steady state, while the back-EMF term $\omega\lambda$ is conveniently compensated in feedforward (Fig. 7). The dynamic response of the $i_\tau$ regulator strongly depends on the factor $b(\lambda, \delta)$ defined in (10) that varies with the working point of the motor. Since $b$ is not constant, a constant proportional gain will give different closed-loop response of $i_\tau$ for different flux situations. For a stable and well-damped response of the regulator, it is suggested to choose the proportional gain with reference to the best-case condition, that is $b = b_{\max}$. The bandwidth of $i_\tau$ will be lower than the rated value $(\omega_b)_\tau$ in most of cases, since it is normally $b < b_{\max}$. The instability region $b < 0$ is avoided by the proper limitation of the $i_\tau$ reference as explained hereafter.

### C. Control Stability $(b > 0)$ and MTPV Boundary

The factor $b$ assumes negative values in part of the flux plane. In case of $b < 0$, the $i_\tau$ control is not stable due to positive feedback, according to Figs. 7 and 8. The $b = 0$ curve is the border of control stability. According to the definition given in (10), $b = 0$ means that the torque derivative with respect to flux phase angle is null. This means that $b = 0$ is the MTPV trajectory [27], as already mentioned in Section III. In flux weakening, the MTPV curve is pursued at high speed for maximum torque control. The instability due to $b < 0$ does not occur if the MTPV trajectory is respected. In the proposed control, the constraint $b = 0$ is fulfilled by the limitation of

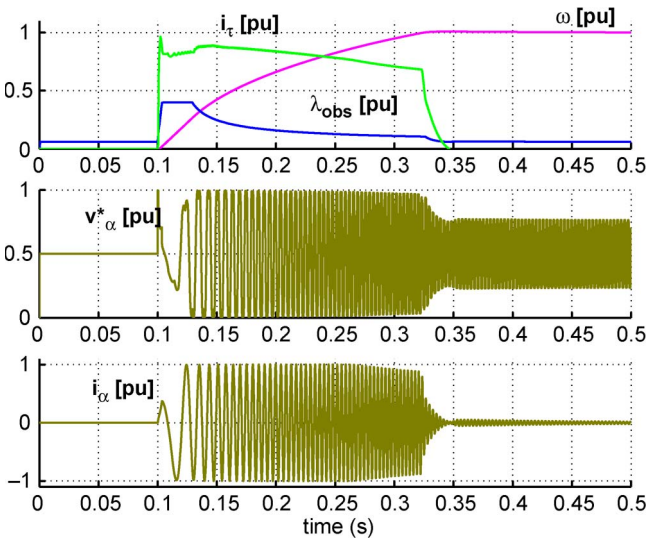


Fig. 8. Simulation-Speed step $0 \div 10\,000$ r/min at no-load. Scale factors: $\omega$: 10 000 r/min/p.u., $\widehat{\lambda}$: 1 V · s/p.u., $i_\tau$: 45 A/p.u., $v_\alpha^*$: 230 V/p.u., $i_\alpha$: 45 A/p.u.

the $i_\tau$ reference value. The limitation of $i_\tau$ corresponds to a limitation of the flux phase angle $\delta$, thus it is possible to constraint the flux vector position inside the MTPV boundary by means of the $i_\tau$ control. The implementation issues of the MTPV limitation block (Fig. 6) are described in Section IV-F.

### D. Flux Reference at Low Speed

The flux reference is set according to the MTPA curve (Fig. 4). The curve has been calculated by means of the motor magnetic characteristics and implemented in a lookup table. In case the accurate motor characterization is not available, simpler control laws are still effective: e.g., in Section V, the MTPA control will be compared with a linear control law. For the maximum torque operation in flux weakening, that is the aim of this paper, the important issue is that point A in Fig. 4 is properly individuated, independently of the $T^* \rightarrow \lambda^*$ control law. Point A can be identified experimentally independently of the knowledge of the complete machine model. Even a constant flux reference equal to $(\lambda)_A$, independently of $T^*$, could be a suitable solution for maximum torque in flux weakening. Nevertheless, the MTPA curve implemented here minimizes the copper and inverter loss at low speed.

### E. Flux Weakening

As the speed increases, the flux reference is limited according to the inverter maximum voltage by means of the simple relationship (11), where the resistive drops are not considered

$$\lambda^* \leq \frac{V_{\max}}{|\omega|}. \tag{11}$$

If the limit $V_{\max}$ is not constant (e.g., battery supplied drive for traction), the flux weakening block can be calculated according to the measured dc-link voltage

$$\lambda^* \leq \alpha \cdot \frac{V_{\rm dc}/\sqrt{3}}{|\omega|} \tag{12}$$

where $V_{\rm dc}$ is the measured dc-link voltage and *alpha* is a constant term, minor or quasi-equal to the unity, that relies for the dynamic voltage margin left to the flux and current regulators.

The resistive term are negligible here as well as in most of cases, but can be included in the flux weakening law (13) suitably simplified by

$$\lambda^* \leq \frac{\sqrt{V_{\max}^2 - (R \cdot i_f)^2} - R \cdot i_\tau}{|\omega|} \tag{13}$$

$$\lambda^* \leq \frac{V_{\max} - R \cdot i_\tau}{|\omega|}. \tag{14}$$

### F. Max Current and MTPV Limitation Blocks

The *max current* block in Fig. 6 limits $i_\tau^*$ according to the amplitude of the measured current

$$i_\tau^* \leq \sqrt{I_{\max}^2 - i_f^2} \tag{15}$$

where $i_f$ is the current component in phase with the flux (4).

The MTPV limitation keeps the flux vector inside the $b > 0$ boundary. The MTPV current limit is calculated according to the maximum current limit (15), augmented or reduced according to the estimated value of $b$ through the proportional gain $k_b$ (Fig. 6). The $k_b$ correction factor has been set to 2 [A] for the drive under test.

The $b$ function is estimated according to (10), based on the simplified magnetic model of the machine (4) where the nonsaturated value of $L_d$ must be used.

The MTPV trajectory varies with the rotor temperature due to the variation of the PM flux term. The working area delimited by the MTPV curve is larger when the rotor temperature is higher, as can be evinced by posing (10) equal to zero. The general advice for having a stable implementation is to use the PM flux value at ambient temperature for the estimation of $b$. In the drive under test, the PM flux is small respect to the total flux, as typical for PMASR-IPM machines, and the temperature effect is weak. In case of an IPM motor with large PM flux and large temperature variations, the exact exploitation of the maximum torque profile cannot obtained in this zone but still the control gives a valid performance with little implementation effort.

Apart from the temperature effect, the other model simplifications have little effect on the MTPV trajectory, at least when the saliency ratio of the motor is sufficiently high (e.g., $\geq 3$): $L_q$ is constant and equal to no-load value because the $d$ current component is small along the MTPV path. $L_d$ is equal to the nonsaturated value minus the cross-saturation effect that reduces the saliency ratio that is anyway high. For machines with low-saliency and high cross saturation, the complete magnetic identification of the motor is necessary for the full torque exploitation at very high speed.

### G. Flux Observer

The control performance relies on the accuracy of the flux observer. The flux observer adopted here is based on the motor

magnetic model at low speed and on back-EMF integration at high speed [10]. Other schemes are possible [11], [12]. Even with the simplified magnetic model (4), where the saturated value of $L_d$ must be used, the response of the observer is fast at any speed and the sensitivity to motor's parameters is very weak:

1) at zero and very low speed, if the flux observer has errors in the estimation of flux amplitude and orientation, the controlled torque is correct but the current is higher then the MTPA one. As the speed increases the error vanishes due to the back-EMF integral contribution. Above the base speed $\omega_A$, the flux estimation is normally correct;
2) the detuning of the motor resistance contributes to the estimation error at low speed.

### H. Effect of Iron Losses at High Speed

Iron losses can be high at elevated speed, in particular for IPM motors of the PMASR type, up to produce a significant reduction of the output torque. Such a negative effect depends on how the machine has been designed and cannot be avoided by the control. Nevertheless, the respect of the MTPV curve in the flux plane [Fig. 4(b)] is independent of the iron loss occurrence. On the contrary, for $d$–$q$-oriented current-controlled drives, the presence of the iron loss equivalent current would shift the MTPV control curve significantly toward the vertical axis of the current plane respect to the one shown in Fig. 4(a), causing more sensitivity to the mechanical position error at high speed.

## V. Simulated and Experimental Results

The field-oriented control is tested on the traction drive of an electric scooter prototype [23]. The IPM motor drive ratings are reported in the Appendix. First of all, the control has been simulated in Matlab Simulink, then implemented on a laboratory rig based on a floating-point microcontroller (ADSP 21060 sharc). Finally, the control has been implemented on the fixed-point DSP (Freescale 56F801) on board of the electric scooter.

### A. Discrete-Time Simulation

The direct field-oriented control is implemented in Matlab Simulink in the form of a discrete-time C- SFunction. The discrete-time SFunction that represents the digital controller is triggered by a timer that accounts for the PWM Interrupt Service Routine of the digital controller. The C- language allows the portability of the control code from the simulation to the experimental implementation. This simulation approach is very powerful for development purposes. The results of the simulations presented throughout this section match the experimental results [Figs. 8 and 11(a)].

### B. Tests on the Laboratory Rig

The laboratory setup consist of an industrial three-phase inverter commanded by a floating-point microcontroller (ADSP 21060 sharc). The voltage and current limits of the inverter are redundant respect to the ones of the scooter drive. The inverter is supplied by the mains through a three-phase rectifier bridge, thus the dc voltage shows a small ripple component at 300 Hz. This will be used in the tests to put in evidence the capability of the control to adapt to a variable dc link, also in real time.

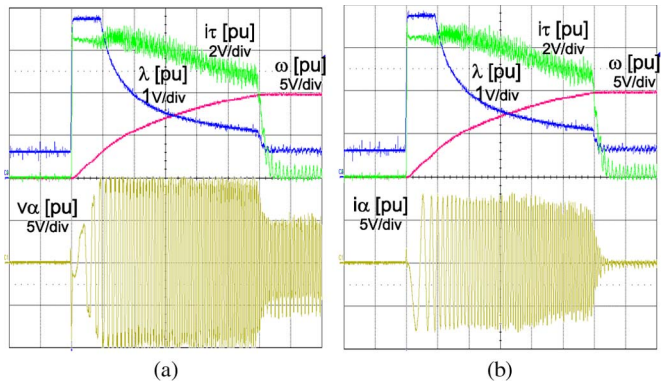


Fig. 9. Experimental speed step $0 \div 10\,000$ r/min at no-load. Scale factors: $\omega$: 10 000 r/min/p.u., $\widehat{\lambda}$: 1 V · s/p.u., $i_\tau$: 45 A/p.u., $v_\alpha^*$: 230 V/p.u., $i_\alpha$: 45 A/p.u. (a) 10 V/1 p.u., 0.1 s/div. (b) 10 V/1 p.u., 0.1 s/div.

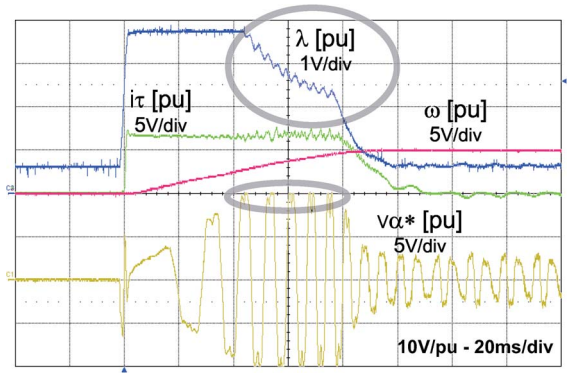


Fig. 10. Experimental speed step $0 \div 5000$ r/min at no-load. The flux reference is adapted to the variable dc link. Scale factors: $\omega$: 10 000 r/min/p.u., $\widehat{\lambda}$: 1 V · s/p.u., $i_\tau$: 45 A/p.u., $v_\alpha^*$: 230 V/p.u., $i_\alpha$: 45 A/p.u.

In the first set of tests (Figs. 9 and 10), the IPM motor drive is speed controlled at no-load. Then, the torque control is tested by drawing the IPM motor by means of a speed controlled primary motor (Figs. 12 and 13).

The drive response to a speed step command from zero to 10 000 r/min is shown in Fig. 9. Constant voltage (subplot a) and phase current (subplot b) are evidenced. In this test, the flux reference in flux weakening refers to a constant $V_{\max}$, according to the (11) formulation.

In Fig. 10, the flux reference in flux weakening is adapted to the measured dc-link voltage, according to (12). The speed step from zero to 5000 r/min is shown. The 300-Hz voltage ripple due to the rectified 50-Hz mains is evidenced in the observed flux trace, while the amplitude of the reference voltage is constant and maximum (trace $v_\alpha^*$).

The trajectory of the flux vector is shown in Fig. 11 for a step transient from zero to 10 000 r/min and then a return step to zero speed. The results are both simulated and experimental. The $A \rightarrow B$ path and part of the MTPV trajectory

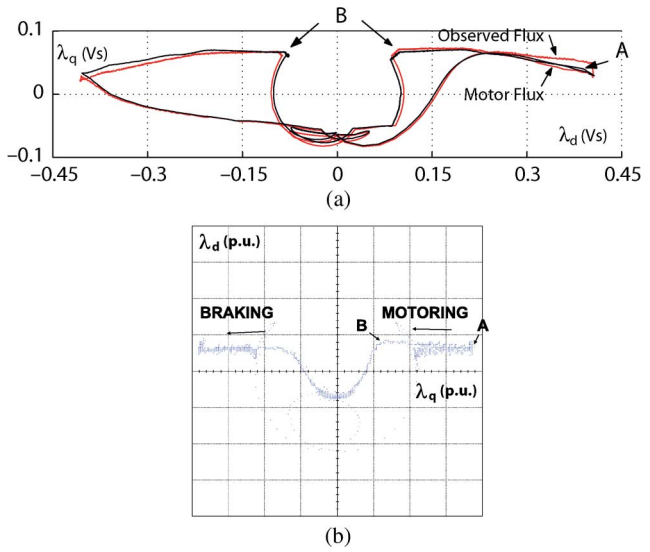


Fig. 11. Maximum torque operation in the full speed range: (right half-plane) speed step 0 → 10 000 r/min and (left half-plane) return step 10 000 → 0 r/min. Full exploitation of the current limit introduced in Fig. 4(b). (a) Simulation. (b) Experimental.

presented in Section III, Fig. 4(b) are exploited by the flux vector.

The flux reference control law at low speed (MTPA) is compared to a simplified linear law [28]. The IPM motor is drawn at constant speed (1000 r/min) by a primary motor and the torque reference is varied slowly from zero to the maximum (Fig. 12). In both cases, the torque is obtained exactly, but with clearly different current values. As already mentioned in Section IV-D, the advantage of the MTPA strategy is to minimize copper loss and inverter conduction loss.

The flux trajectory is shown in Fig. 13 for different speeds. In this case, the IPM motor is drawn at different constant speeds by a primary motor and the torque reference is varied from zero to maximum torque. The circular trajectories in the flux plane represent a constant flux amplitude and then constant voltage operation at the various speeds. At low torque, the flux trajectories follow the MTPA curve at all speeds.

### C. Tests on the Electric Scooter

A picture of the prototype electric scooter [23] is shown in Fig. 14. The vehicle specifications are in the Appendix. The digital controller is an industrial fixed-point DSP (Freescale 56F801). The scooter frame is a commercial one where the electric power-train and the Li-Ion battery pack for traction have been housed. The throttle lever has been adapted to set the torque reference of the traction drive by means of a potentiometer. Dealing with the vehicle brakes, the left brake lever is dedicated to the electric braking, while the right lever is unmodified and actuates the front mechanical brake. For urban vehicles such as the prototype scooter, regenerative braking can fulfill most of the required braking needs. If most of the braking power is regenerated by a proper electric braking strategy, the vehicle range considerably rises. In the scooter prototype, the electric braking is managed into two different modes: the

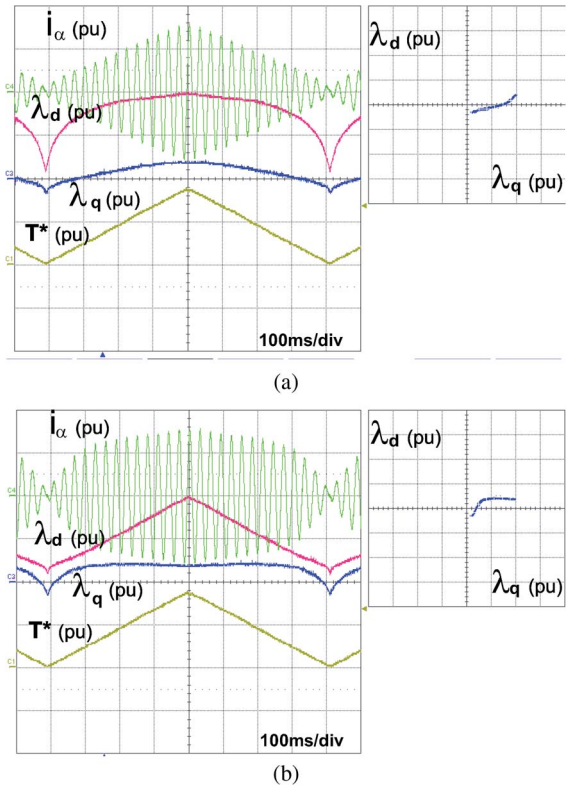


Fig. 12. Zero to maximum torque at low speed: MTPA versus linear control law. Scale factors: 0.2 V · s/div, 20 N · m/div, 22.5 A/div. (a) MTPA control law. (b) Simplified linear control law.

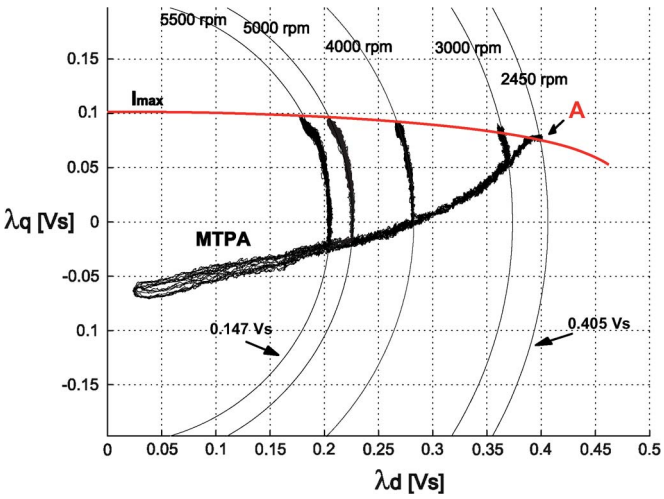


Fig. 13. Zero to maximum torque at different speeds. The MTPA trajectory is followed unless the voltage limit is reached.

*engine brake* mode, a smooth braking action at the release of the throttle lever, and the *lever brake* mode that exploits the full IPM motor torque to brake the scooter when the left brake lever is actioned.

In Fig. 15, an operating cycle of the scooter is presented. The observed flux and $i_\tau$ current component of the IPM motor drive are reported in the bottom plot, while the measured motor speed and the reference torque are in the top plot. The scooter is operated with the traction wheel lifted from the floor for practical reasons of data collection. In the presented cycle then, the load

Fig. 14. Electric scooter prototype.

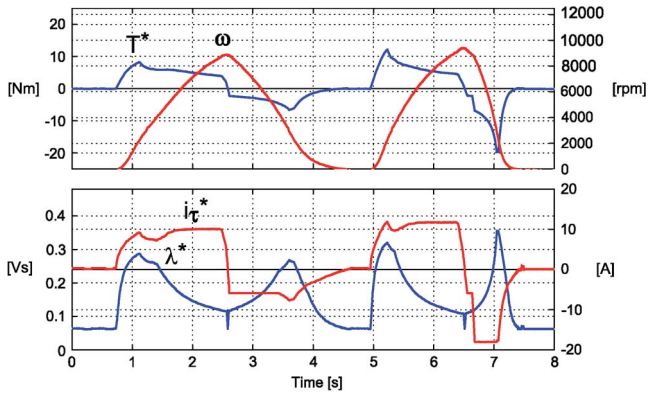


Fig. 15. Electric scooter acceleration–deceleration cycle. The traction wheel is released from the ground, only electric braking is used.

is represented by the inertia of the power-train itself plus the transmission belt and the traction wheel. Only electric braking is used in the test. After the first acceleration (time 0.8 s ÷ 2.6 s), the throttle lever is released and the vehicle decelerates in the *engine brake* mode (time 2.6 s ÷ 4 s). There is a second acceleration (time 5.0s ÷ 6.5 s) that is a little faster than the first one. Finally, (time 6.5 s ÷ 7.0 s), a regenerative braking at full torque is actuated by the driver by means of the brake leverage. The evaluation of the motor speed response over the entire operating range (0 ÷ 10 000 r/min) confirms the feasibility of the proposed control.

## VI. Conclusion

The direct flux control of an IPM motor drive in the field-weakening region has been presented, simulated, and tested. The drive under test is the 7-kW IPM-PMASR motor drive of a prototype electric scooter designed for urban mobility. The direct flux control is implemented in the stator flux-oriented reference frame. The flux reference is individuated by means of a flux observer. The control takes into account the voltage and current limits with simple computational solutions, with no need of an accurate characterization of the IPM motor. The voltage limit can be adapted to a variable dc link with no modification of the algorithm. Experimental tests on a laboratory rig and on the scooter prototype confirm the feasibility of the proposed control.

TABLE I
IPM Drive Ratings

| MOTOR DATA | | | |
|---|---|---|---|
| Cont. Power | $P_{nom}$ | $kW$ | 7 |
| Peak Power | $P_{max}$ | $kW$ | 10 |
| Base Speed | $\omega_A$ | $rpm$ | 2450 |
| Max Speed | $\omega_{max}$ | $rpm$ | 10000 |
| Stator resistance | $R$ | $\Omega$ | 0.3 |
| Inertia (Motor) | $J$ | $kgm^2$ | $4.6\ 10^{-3}$ |
| INVERTER DATA | | | |
| Current | $I_{max}$ | $Apk$ | 35 |
| Voltage (star) | $V_{max}$ | $Vpk$ | 210 |

TABLE II
Scooter Prototype Ratings

| | | | |
|---|---|---|---|
| Total weight | 2 passengers | $kg$ | 320 |
| Max Speed | | $km/h$ | $90 \div 100$ |
| Gradability | | | 25% |
| Range | @$50km/h$ | $km$ | 130 |
| Range | @$90km/h$ | $km$ | 60 |

## Appendix
## IPM Drive and Electric Scooter Ratings

The ratings of the IPM motor drive are summarized in Table I. The ratings of the electric scooter are summarized in Table II.

## References

[1] T. M. Jahns, G. B. Kliman, and T. W. Neumann, "Interior permanent magnet synchronous motors for adjustable speed drives," *IEEE Trans. Ind. Appl.*, vol. IA-22, no. 4, pp. 738–747, Jul. 1986.

[2] A. Fratta, A. Vagati, and F. Villata, "On the evolution if AC machines for spindle drives applications," *IEEE Trans. Ind. Appl.*, vol. 28, no. 5, pp. 1081–1086, Sep./Oct. 1992.

[3] W. L. Soong and T. J. E. Miller, "Field-weakening performance of brushless synchronous AC motor drives," *Proc. Inst. Elect. Eng.—Electr. Power Appl.*, vol. 141, no. 6, pp. 331–340, Nov. 1994.

[4] A. Fratta, A. Vagati, and F. Villata, "Design criteria of an IPM machine suitable for field-weakening operation," in *Proc. Int. Conf. Elect. Mach.*, 1990, pp. 1059–1065.

[5] N. Bianchi and S. Bolognani, "Unified approach to the analysis and design of an AC motor drive for flux-weakening operations," in *Conf. Rec. 33rd IEEE IAS Annu. Meeting*, Oct. 1998, vol. 1, pp. 95–102.

[6] S. R. Macminn and T. M. Jahns, "Control techniques for improved high-speed performance of interior PM synchronous motor drives," *IEEE Trans. Ind. Appl.*, vol. 27, no. 5, pp. 997–1004, Sep./Oct. 1991.

[7] S. Morimoto, T. Ueno, M. Sanada, Y. Takeda, and T. Hirasa, "Variable speed drive system of interior permanent magnet synchronous motors for constant power operation," in *Proc. IEEE Power Convers. Conf.*, 1993, pp. 402–407.

[8] J. Kim and S. Sul, "Speed control of interior permanent magnet synchronous motor drive for the flux weakening operation," *IEEE Trans. Ind. Appl.*, vol. 33, no. 1, pp. 43–48, Jan./Feb. 1997.

[9] J. Wai and T. M. Jahns, "A new control technique for achieving wide constant power speed operation with an interior PM alternator machine," in *Conf. Rec. IEEE IAS Annu. Meeting*, 2001, vol. 2, pp. 807–814.

[10] A. Vagati, M. Pastorelli, G. Franceschini, and V. Drogoreanu, "Digital observer-based control of synchronous reluctance motors," in *Conf. Rec. IEEE IAS Annu. Meeting*, 1997, vol. 1, pp. 629–636.

[11] K.-H. Kim, S.-K. Chung, G.-W. Moon, I.-C. Baik, and M.-J. Youn, "Parameter estimation and control for permanent magnet synchronous motor drive using model reference adaptive technique," in *Proc. 21st Annu. IEEE IECON*, Nov. 1995, vol. 1, pp. 387–392.

[12] Y. Jeong and S. K. Sul, "Adaptive flux observer with on-line inductance estimation of an IPMSM considering magnetic saturation," in *Conf. Rec. IEEE PESC*, 2005, pp. 2467–2473.

[13] S.-H. Kim and S.-K. Sul, "Maximum torque control of an induction machine in the field weakening region," *IEEE Trans. Ind. Appl.*, vol. 31, no. 4, pp. 787–794, Jul./Aug. 1995.

[14] F. Briz, A. Diez, M. W. Degner, and R. D. Lorenz, "Current and flux regulation in field-weakening operation [of induction motors]," *IEEE Trans. Ind. Appl.*, vol. 37, no. 1, pp. 42–50, Jan./Feb. 2001.
[15] M.-H. Shin, D.-S. Hyun, and S.-B. Cho, "Maximum torque control of stator-flux-oriented induction machine drive in the field-weakening region," *IEEE Trans. Ind. Appl.*, vol. 38, no. 1, pp. 117–122, Jan./Feb. 2002.
[16] P. Guglielmi, M. Pastorelli, G. Pellegrino, and A. Vagati, "Position sensorless control of permanent-magnet-assisted synchronous reluctance motor," *IEEE Trans. Ind. Appl.*, vol. 40, no. 2, pp. 615–622, Mar./Apr. 2004.
[17] H. F. Hofmann, S. R. Sanders, and A. EL-Antably, "Stator-flux-oriented vector control of synchronous reluctance machines with maximized efficiency," *IEEE Trans. Ind. Electron.*, vol. 51, no. 5, pp. 1066–1072, Oct. 2004.
[18] S. P. Das and A. K. Chattopadhyay, "Observer-based stator-flux-oriented vector control of cycloconverter-fed synchronous motor drive," *IEEE Trans. Ind. Appl.*, vol. 33, no. 4, pp. 943–955, Jul./Aug. 1997.
[19] M. Bilewski, A. Fratta, L. Giordano, A. Vagati, and F. Villata, "Control of high-performance interior permanent magnet synchronous drives," *IEEE Trans. Ind. Appl.*, vol. 29, no. 2, pp. 328–337, Mar./Apr. 1993.
[20] L. Qinghua, A. M. Khambadkone, and M. A. Jabbar, "Direct flux control of interior permanent magnet synchronous motor drives for wide-speed operation," in *Proc. 5th Int. Conf. PEDS*, Nov. 2003, vol. 2, pp. 1680–1685.
[21] X. Xu and D. Novotny, "Selection of the flux reference for induction machine drives in the field weakening region," *IEEE Trans. Ind. Appl.*, vol. 28, no. 6, pp. 1353–1358, Nov./Dec. 1992.
[22] G. S. Buja and M. P. Kazmierkowski, "Direct torque control of PWM inverter-fed AC motors—A survey," *IEEE Trans. Ind. Electron.*, vol. 51, no. 4, pp. 744–757, Aug. 2004.
[23] E. Armando, P. Guglielmi, M. Martino, and M. Pastorelli, "Big electric scooter: An experience from lab to the road," in *Proc. 3rd IEEE ICIEA*, Jun. 2008, pp. 1680–1684.
[24] A. Vagati, M. Pastorelli, and G. Franceschini, "Effect of magnetic cross-coupling in synchronous reluctance motors," in *Proc. PCIM*, Nurnberg, Germany, 1997, vol. IM, pp. 279–285.
[25] S. Morimoto, M. Sanada, and Y. Takeda, "Performance of PM assisted synchronous reluctance motor for high efficiency and wide constant power operation," in *Conf. Rec. IEEE IAS Annu. Meeting*, 2000, vol. 1, pp. 509–514.
[26] S. Morimoto, Y. Takeda, T. Hirasa, and K. Taniguchi, "Expansion of operating limits for permanent magnet motor by current vector control considering inverter capacity," *IEEE Trans. Ind. Appl.*, vol. 26, no. 5, pp. 866–871, Sep./Oct. 1990.
[27] S. Morimoto, "IPM vector control and flux weakening," in *Conf. Rec. IEEE IAS Annu. Meeting—Tutorial Course Notes—Design, Analysis, and Controlof Interior PM Synchronous Machines*, 2004, pp. 8–1–8–35.
[28] G. Pellegrino, E. Armando, and P. Guglielmi, "Field oriented control of IPM drives for optimal constant power operation," in *Proc. Eur. Conf. Power Electron. Appl.*, Sep. 2007, pp. 1–10.
[29] A. Fratta, A. Vagati, and F. Villata, "Permanent magnet assisted synchronous reluctance drive for constant power applications: Comparative analysis of control requirements," in *Proc. Power Convers. Intell. Motion*, 1992, vol. IM, pp. 187–195.
[30] N. Bianchi and S. Bolognani, "Magnetic models of saturated interior permanent magnet motors based on finite element analysis," in *Conf. Rec. IEEE IAS Annu. Meeting*, 1998, vol. 1, pp. 27–34.
[31] M. F. Rahman, L. Zhong, and K. W. Lim, "A direct torque controlled interior permanent magnet synchronous motor drive incorporating field weakening," *IEEE Trans. Ind. Appl.*, vol. 34, no. 6, pp. 1246–1253, Nov./Dec. 1998.
[32] B. Stumberger, G. Stumberger, D. Dolinar, A. Hamler, and M. Trlep, "Evaluation of saturation and cross-magnetization effects in interior permanent-magnet synchronous motor," *IEEE Trans. Ind. Appl.*, vol. 39, no. 5, pp. 1264–1271, Sep./Oct. 2003.
[33] Z. Xu and M. F. Rahman, "An improved stator flux estimation for a variable structure direct torque controlled IPM synchronous motor drive using a sliding, observer," in *Conf. Rec. 40th IEEE IAS Annu. Meeting*, Oct. 2005, vol. 4, pp. 2484–2490.
[34] T. J. E. Miller, M. Popescu, C. Cossar, and M. McGilp, "Performance estimation of interior permanent-magnet brushless motors using the voltage-driven flux-MMF diagram," *IEEE Trans. Magn.*, vol. 42, no. 7, pp. 1867–1872, Jul. 2006.
[35] G. Pellegrino, E. Armando, and P. Guglielmi, "Optimal exploitation of the constant power region of IPM drives based on field oriented control," in *Conf. Rec. 42nd IEEE IAS Annu. Meeting*, Sep. 2007, pp. 1335–1340.

**Gianmario Pellegrino** (M'06) received the M.Sc. and Ph.D. degrees in electrical engineering from the Politecnico di Torino, Turin, Italy, in 1998 and 2002, respectively.

He was a Guest Researcher at Aalborg University, Denmark, in 2002. Since 2002, he has been with the Department of Electrical Engineering, Politecnico di Torino, first as Research Associate and, since 2007, as an Assistant Professor. He has been teaching courses on power electronics and electric drives. He is involved in research projects for the public sector and for private groups. He has more than 30 technical papers and one international patent. His areas of interest are electric drives, namely, in motor design and digital control. He works in the fields of electric traction and the design of direct-drive generators for wind energy production.

**Eric Armando** was born in Cuneo, Italy, in 1974. He received the M.Sc. and Ph.D. degrees in electrical engineering from the Politecnico di Torino, Turin, Italy, in 2002 and 2008, respectively.

He is currently with the Politecnico di Torino as a Research Assistant. He has been in charge of national research projects, funded by the Italian Research Ministry board, in the field of ac drives. His fields of interest include power electronics and high-performance ac motor drives.

**Paolo Guglielmi** (M'07) was born in Imperia, Italy, in 1970. He received the M.Sc. degree in electronic engineering and the Ph.D. degree in electrical engineering from the Politecnico di Torino, Turin, Italy, in 1996 and 2001, respectively.

In 1997, he joined the Department of Electrical Engineering, Politecnico di Torino, where he has been a Researcher since 2002. He has authored several papers published in technical journals and conference proceedings. His fields of interest include power electronics, high-performance servo-drives, and computer-aided design of electrical machines.

Dr. Guglielmi is a Registered Professional Engineer in Italy.